Maral Ansari, Lizhao Song, Pei-Yuan Qin, Stephanie L. Smith, and Y. Jay Guo

Advances in Multibeam Flat GRIN Lens Antennas

A promising 3D-printed design.

xxxxx

High-gain multibeam antennas are indispensable components in high-speed satellite communication (SatCom) systems. They have the ability to produce multiple directive beams that can cover a predefined angular range. Among different multibeam antennas, gradient-index (GRIN) flat lenses serve as a promising technology to realize multibeam radiation with their advantages of low profile, easy installation, low cost, high efficiency, and a wide beam coverage. This article describes the recent advances in GRIN lens antennas. In particular, this article presents a novel 3D-printed multibeam GRIN lens antenna. The design offers a broad 2D angular coverage of ±45°. It maintains a scanning loss of less than 2.4 dB and sidelobe levels (SLLs) below –10 dB. The antenna also achieves a high aperture efficiency of up to 60% across the 12–15-GHz frequency band.

Digital Object Identifier 10.1109/MAP.2025.3588059

INTRODUCTION

High-gain multibeam antennas have emerged as key enablers in modern SatCom systems, meeting the increasing demand for high-capacity, reliable, and adaptable connectivity solutions. These antennas enable satellite systems to serve multiple users simultaneously, each located in different geographic areas, which is critical for ensuring seamless coverage across large and often remote regions. The ability to focus energy into multiple narrow beams allows for efficient use of frequency resources, which is essential for managing the increasingly congested radio spectrum in modern SatCom systems. This efficiency directly contributes to higher data transmission rates, improved network capacity, and reduced interference.

In the context of SatCom, high-gain multibeam antennas are vital for facilitating long-range communications with wide spatial coverage, supporting diverse industrial applications, such as telecommunications, broadcasting, and disaster recovery. Additionally, multibeam antennas are crucial for the next generation

of satellite networks, particularly those involving low-Earth orbit (LEO) constellations, where their ability to dynamically switch between beams improves network responsiveness and service continuity. As satellite networks evolve, especially with the integration of LEO and medium-Earth orbit constellations, high-gain multibeam antennas will continue to play an essential role in ensuring high performance, minimal latency, and optimal spectrum utilization across global communication networks [1].

Typical methods to produce multiple directive beams include circuit-type beamforming networks [2], [3], [4], such as the Butler matrix [5], [6], [7], Blass matrix [8], [9], Nolen matrix [10], [11], and generalized joined coupler matrix [12], [13]. Additionally, quasi-optical multibeam antenna systems [14], including reflectors [15], [16], metasurface structures [17], [18], transmitarrays [19], [20], reflectarrays [21], [22], and different types of lenses [23], [24], are also employed. Among these technologies, lens antennas are emerging as a promising solution for high-gain multibeam radiation owing to their favorable features, such as a broad field of view, a wide bandwidth, and a simple feeding network.

Lenses, like reflectors, are a type of aperture antenna whose gain increases with the aperture's effective area. They can eliminate aperture blockage and allow control over the electromagnetic wave propagation. This can be achieved by using shaped structures [25], [26], [27] or by adjusting the refractive index distribution [28]. Homogeneous lenses use a single dielectric material with a shaped surface. By contrast, inhomogeneous lenses have a nonuniform refractive index distribution [29], [30], [31].

Lens antennas are traditionally used to enhance antenna gains by transforming spherical wavefronts into planar ones. Recently, they have attracted significant commercial interest, particularly for beam scanning and multibeam applications. Multiple beams can be concurrently generated through the integration of lenses with multiple feeding antenna elements [32]. Beam-scanning and multibeam lens antennas have been explored using various types of lenses. These include traditional spherical Luneburg lenses as well as their transformed, compressed, and flat shapes combined with feed arrays [33], [34]. Other types involve integrated lens antennas made of shaped dielectrics with multiple feed elements [35], [36]. Profiled and flat lenses using solid dielectric materials or GRIN structures have also been investigated [37], [38], [39].

This renewed focus is driven by advancements in compact lens design and the development of artificial dielectrics and metamaterials [34], [40], which has facilitated the manufacture of lenses [37], [40], making them more accessible for practical use. Over the last decade, numerous 3D-printed lens designs have been reported in the literature [40], [43], [44], [45], [46]. While these designs inherently feature spherical configurations that enable high-gain performance and well-formed multibeam coverage, their bulky structure complicates their integration with communication platforms. Therefore, planar 3D-printed lenses with more degrees of design freedom have attracted significant attention and been well examined [47].

In this article, the recent advancements of planar GRIN lenses are discussed. These lenses are similar to other beam-collimation antennas, such as Fresnel zone plate lenses [48], [49], [50], superstrate and metasurfaces [51] as well as transmitarrays [52], [53], [54], except that the GRIN lens follows the optical rules enabling larger bandwidths and higher efficiencies [55]. The GRIN profile of the lens is determined by analyzing the ray path through the lens medium.

In the following sections, the operating mechanism of GRIN lenses is described, and some of the reported GRIN lens antennas are reviewed. A flat GRIN lens with a low scanning loss and a high aperture efficiency is introduced. The lens design is based on the bifocal analysis method. The flat lens is used to realize 2D wide-angle multibeam radiation. In comparison to bulky spherical lenses, the proposed flat lens design has a smaller weight. It can be integrated with planar platforms without protruding from the surface, meeting aerodynamic requirements for airborne or spaceborne systems. The aperture of the lens can be implemented using low-cost technologies, such as printed circuit board (PCB) or 3D printing. The multibeam antenna prototype is tested with good agreement between the simulated and measured results.

THE GRIN LENS

The analytical refractive index profile of the GRIN lens is reported in [56] and is shown in Figure 1. Because of the desired plane wavefront at the exit of the lens, the two different ray paths, which travel through free space and the lens with radial refractive index values, respectively, should have equal phase delays. The condition is given by

$$\int_{P_1}^{P_2} n\mathrm{d}z = n_{\max} d - (P - F) \tag{1}$$

where P_1 is an arbitrary incident point on the lens for the wave with an incident angle of θ, P_2 is the corresponding exit point on the output aperture, $n_{\max}$ is the refractive index at the center of the lens, n is the refractive index of a generic point in the lens, and P is the focal distance of point P_1. Assuming that the refractive index varies linearly between P_1 and P_2, and the lens is thin, one can obtain the expression for n in terms of θ [56]:

$$\frac{d}{F}\left(n^2 - \frac{2}{3}\sin^2\theta\right) = \sqrt{n^2 - \sin^2\theta}\,\left(n_{\max}\frac{d}{F} - \sec\theta + 1\right). \tag{2}$$

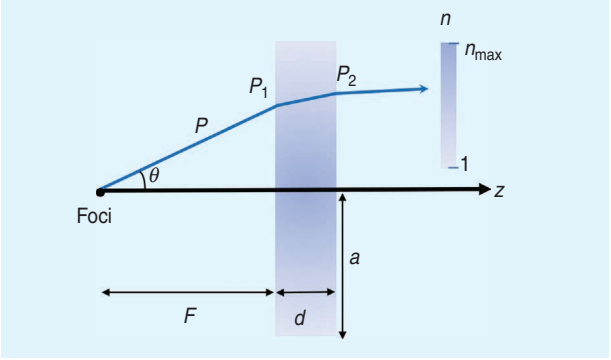

FIGURE 1. GRIN lens profile with ray path through the lens.

The GRIN profile is determined based on the values of focal length F, thickness d, and diameter $2a$. The ratio F/a corresponds to the gain and the scan angle, and the d/a ratio determines the refractive index and n_{max}. In particular, a larger a corresponds to higher gains, and a smaller F/a ratio would allow lower profile designs with some compromise to the radiation performance [57]. One of the drawbacks of GRIN flat lenses is their limitation in implementation of the continuously graded index variation, which is required to achieve a high aperture efficiency. Usually, a discrete graded index profile can be realized. However, this will lead to a phase error, resulting in a lower aperture efficiency.

A closed-form solution is reported for radial GRIN lenses with a novel formulation to reduce the phase error of the lens profile [57]. The geometry of the lens is shown in Figure 2. The feed is positioned at a distance F from the lens, characterized by a refractive index profile $n(\rho)$. The formulation is based on the nonlinear integral equation representing the equalization of all of the optical ray-path lengths. The equation of the ray path is calculated by integrating along ρ, which is a generic radius. Since ρ_{in} is arbitrary, one can substitute ρ_{in} with ρ. Based on this method, the refractive index distribution of the lens can be calculated from (3), where the value of c (the parameter to be optimized) is found from a least mean-square optimization method. This method can achieve a refractive index profile of the lens that results in a high aperture efficiency in a large bandwidth with negligible phase error at the output interface for a vast range of F and d. It allows the design of thick lenses of low n_{max} without matching layers as well as very thin lenses of high refractive index with the use of matching layers to avoid mismatch. This design can realize an aperture efficiency of up to 80% considering the optimum F and d values:

$$n(\rho) = \sqrt{\left(n_{\max} + \frac{F - \sqrt{F^2 + \rho^2}}{d}\right)^2 + c\frac{\rho^2}{F^2 + \rho^2}}. \qquad (3)$$

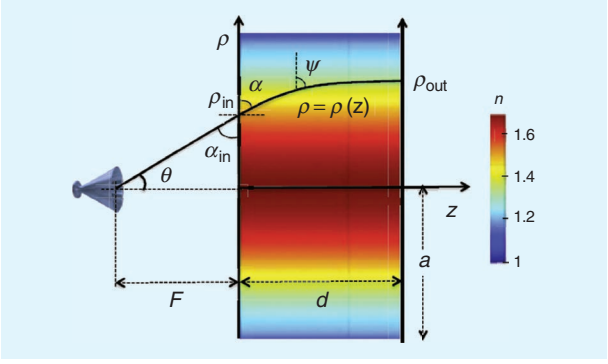

FIGURE 2. Geometry of the lens and geometrical parameters [57].

A flat-layered collapsible GRIN lens antenna operating at the Ku band is reported in [58], where the lens's graded index is implemented by multilayer microstrip closed square-ring units of variable sizes distributed on both sides of thin planar dielectric substrates. The lens GRIN profile follows (2). The main contribution of the work is the air gap between adjacent dielectric layers, which allows the lens to be stowed and compressed, resulting in a low profile, and then deployed to an operational configuration once the air separation is fixed. The final lens prototype has a diameter of 5λ at 13.5 GHz, a height of collapsed and operational arrangement equal to 0.19λ and 0.92λ, respectively, and a gain of 22.5 dBi for the boresight beam with the SLL below –18.8 dB. The unit cell, as shown in Figure 3(a), is a square-ring patch printed on dielectric substrates. This fabricated lens in the storage configuration is shown in Figure 3(b).

As mentioned earlier, GRIN lenses can also radiate multiple beams. The multibeam performance of a wideband flat GRIN lens antenna is investigated in [59]. An array of five waveguides is placed at the focal plane of a 3D-printed perforated flat lens operating between 45 and 110 GHz. Five beams are generated covering an azimuthal elevation range of $\pm 30^{\circ}$ with realized gains of 17–20 dBi corresponding to an aperture efficiency of 19%–36%. The SLL is below –5 dB at beams pointing to the widest angles. The geometry of the flat lens-based multibeam antenna system is shown in Figure 4. Different beams are created by switching the array elements in the xy plane. The

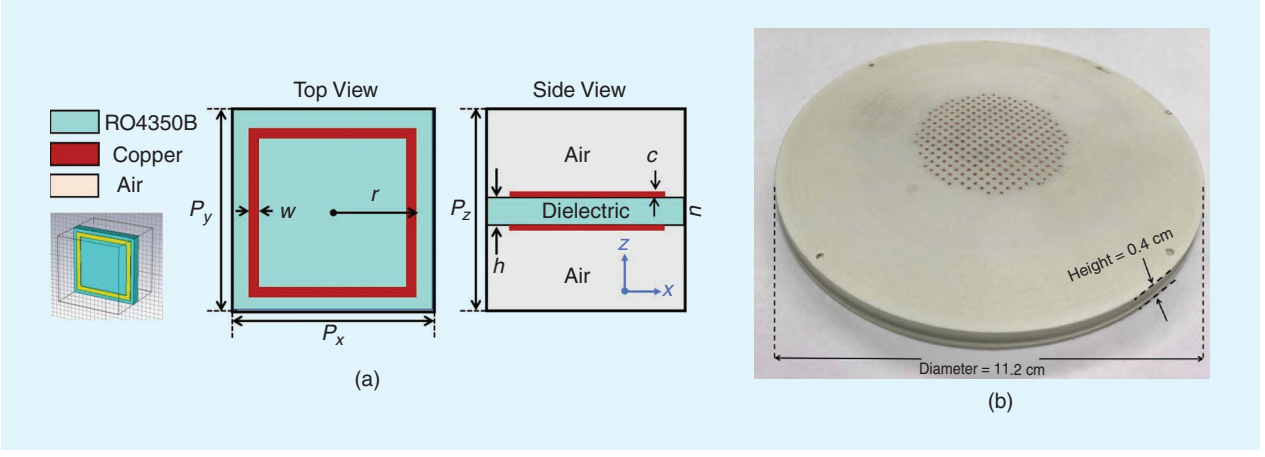

FIGURE 3. (a) Unit cell employed for the GRIN lens design. (b) Folded lens when collapsed (stored) [58].

fabricated 3D-printed lens prototype features holes with a diameter of 1 mm. The hole-to-hole spacing (s) varies across four distinct layers, with a d/s ratio ranging from 0.58 to 0.81.

A practical implementation of a dielectric flat lens antenna is presented in [60]. The final lens prototype is obtained with 1200 carbide drilling of 0.2- and 0.5-mm-diameter holes on Rogers TMM6 substrate making up a discrete GRIN profile of six layers. A WR-15 rectangular waveguide is used to efficiently illuminate the lens, achieving a 14.8-dB edge taper in the H-plane. It is positioned in an array along the x direction, with a 2-mm step from rho = 8 mm to rho = 8 mm, enabling a beam-scanning range of $\pm 48^\circ$ (as shown in Figure 5, rho is the feed offset from the focus along the x direction). H-plane radiation patterns are plotted in Figure 5 for two different frequencies. The gain ranges from 13.7 to 18.3 dB at 60 GHz with SLLs better than –7 dB and from 15.4 to 18.9 dB at 77 GHz with SLLs better than –3.5 dB. The aperture efficiency is between 9.5% to 27.5%. It is seen that the lens antenna performance is deteriorated at large scanning angles, resulting in high SLLs and low aperture efficiencies. A multibeam performance of this lens antenna can be obtained by placing several feeds as an array along the focal plane of the lens.

Recently, a compact low-cost 3D-printed dielectric perforated flat GRIN lens with integrated dual-circular polarizer at the W band was reported in [61]. The geometry of the lens, integrated polarizer, and feed is given in Figure 6(a). Beam scanning of the lens antenna is achieved by displacing a square waveguide feed on the focal plane of the lens, as sketched in Figure 6(b). The corresponding radiated beams cover a scan range of $\pm 30^\circ$ in both the azimuth and elevation planes. The measured directivity values change from 23.5 to 23.8 dB, and the aperture efficiency for a broadside beam stays between 90.32% and 57.34%.

The aforementioned GRIN lenses enable multibeam performance by placing multiple feeds along a straight feed trajectory or mechanical beam scanning by sliding a feed antenna along a straight trajectory. As a result, at wider scanning angles, the beam deteriorates noticeably because of spillover losses or higher errors occurring in the refractive index profile. A method to enhance the beam-scanning performance of flat lens antennas is proposed in [62], where a set of feed-correction lenslets (FCL) is used to radiate squint beams toward the lens center to improve the scan collimation by reducing the spillover losses. As a result, a wider beam range of $\pm 53^\circ$ with a peak aperture efficiency of 74% at 18 GHz and a scan loss of less than 5.5 dB is achieved. This concept is shown in Figure 7, where translated feed positions for ports 1–5 are also shown and the GRIN profile of the FCLs for feed position 5 is provided. However, it is very challenging to achieve a 2D multibeam design because of the large volume of the FCL-assisted horns. Even for the 1D

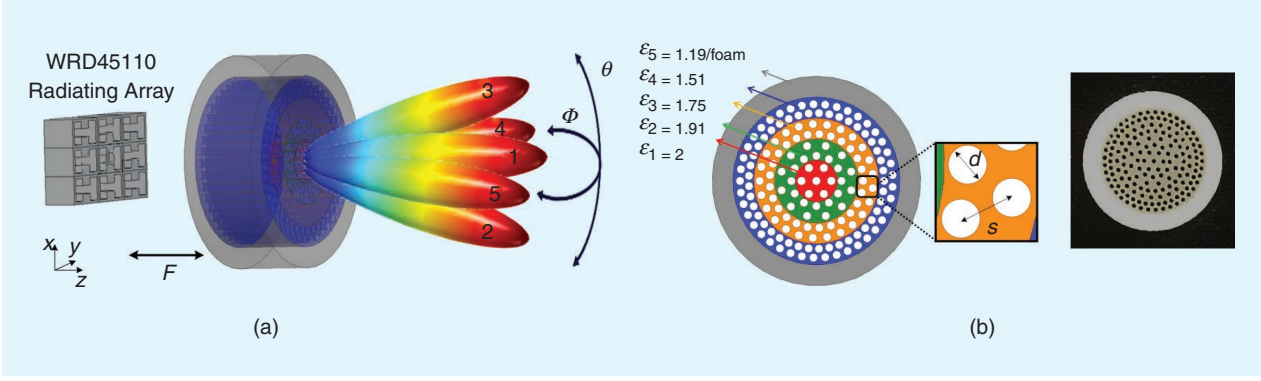

FIGURE 4. (a) Illustration of the switched lens-based multibeam antenna system. (b) Simulated model and 3D-printed prototype of the five-layer perforated flat lens [59].

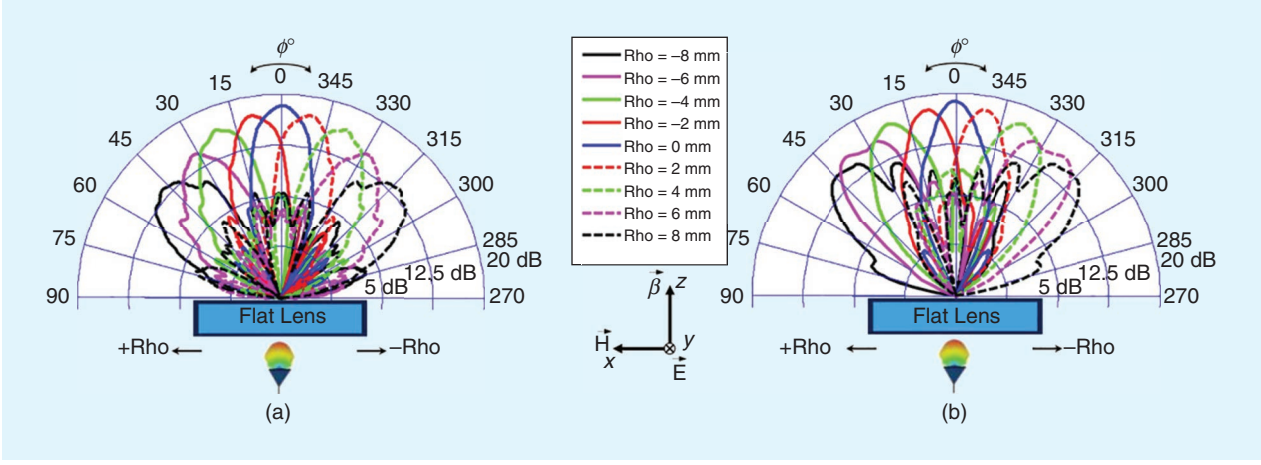

FIGURE 5. H-plane radiation patterns for different feeding positions (a) 60 GHz and (b) 77 GHz [60].

multibeam design, there is less flexibility on the control of the crossover of multiple beams as physically two adjacent horns cannot be overlapped.

In [63], the authors proposed a GRIN variation to design a multifocal lens that enables 2D beam scanning over a wide field of view with low scan losses and high aperture efficiencies. The lens configuration is given in Figure 8.

New methods based on bifocal analysis are found to determine the refractive index profile of the lens as well as the feed positions along a circular feed locus to enable independent wide-angle multibeam radiation. A 2D multibeam GRIN lens has been successfully developed. It is fed by 13 feed antennas, each consisting of a 2×2 patch array. These feeds are positioned along the focal planes in the xz and yz planes. Wide-angle multibeam radiation has been obtained with a beam coverage of around $\pm 45^{\circ}$ in both the xz and yz planes. The 3D geometry of the feed is implemented for a better scanning performance. Although the feeds are along a circular feed locus leading to a larger focal area, the lens itself has a flat structure, which uses less material and has a lighter weight compared to spherical Luneburg lenses with their bulky and heavy structures. The lens aperture is designed using multilayer metasurfaces. The required refractive index profile of the lens is obtained by

$$n(r, \phi_1) = n_{\max} - \frac{\sqrt{l_0^2 + r^2(1 - \cos\phi_0 \sin\beta)^2} - l_0}{d/\cos\beta} \tag{4}$$

where β is the maximal radiation angle (in this case $\pm 45^{\circ}$), and l_0 is the focal length for the feed at this angle. The minimum refractive index on the edge of the lens is 1, i.e., $n(a, \pm \pi/2) = 1$, and the constant $n_{\max}$ is calculated as

$$n_{\max} = 1 + \frac{\sqrt{l_0^2 + a^2} - l_0}{d/\cos\beta}. \tag{5}$$

Based on the theory reported in [63], here we present the design and fabrication of a multibeam GRIN lens antenna with a considerable improvement in the oblique beams. Because of the similar lens diameters and feed antennas, this work presents a similar performance in terms of gain and bandwidth. However, it develops an all-dielectric unit cell, enabling the lens implementation using 3D-printing technology. The all-dielectric design of the lens offers advantages that allow the entire structure to be seamlessly integrated into a single 3D printing, resulting in simplified manufacturing. It also provides a lower cost and a lower scanning loss compared to lenses designed using PCB technology. More details of the design are given in the following section.

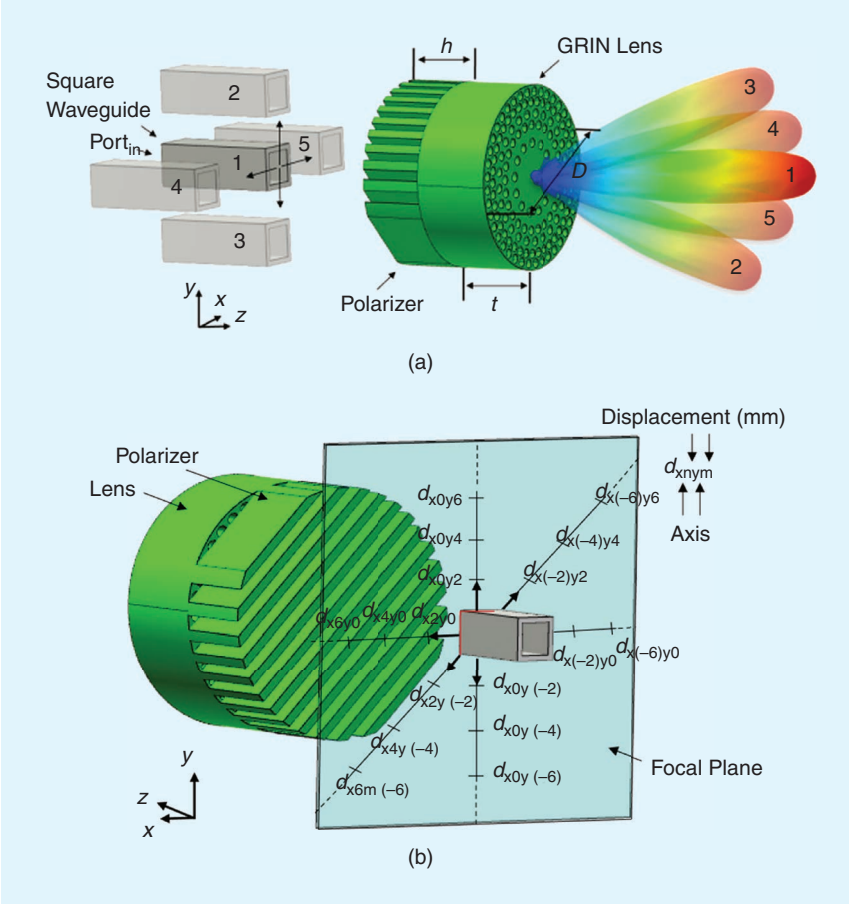

FIGURE 6. (a) Geometry of dual-circular polarizer GRIN flat lens with integrated polarizer fed by a square waveguide feed. (b) Coordinate system for feed displacements along lens focal plane [61].

3D-PRINTED 2D MULTIBEAM FLAT GRIN LENS

In this section, a 3D-printed flat GRIN lens antenna with a diameter of $2a = 110$ mm $(5\lambda_0)$ and a thickness of $d = 22$ mm $(1\lambda_0)$ operating from 12 to 15 GHz is presented, where λ_0 is the wavelength in free space at 13.5 GHz.

3D-PRINTED 2D MULTIBEAM FLAT GRIN LENS DESIGN

The required refractive index distribution of the GRIN lens is obtained using (4). The lens aperture is divided into six radial sections and 36 azimuthal sectors. This segmentation helps achieve an approximately linear phase across the lens aperture. The desired phase distribution is determined by an arc of the circular feed locus. This enables the generation of oblique beams at extreme scanning angles (in this case, $\pm 45^{\circ}$). Once the GRIN profile and the corresponding focal point for the maximum radiation beam are determined, the optimal focal length for the boresight beam is found by adjusting the feed position along the z-axis to minimize the phase error on the aperture.

The calculated required refractive index of the lens is given in Figure 9(a) with a variation range from 1 to the maximum (n_{max}) of 1.4 corresponding to the center of the lens. This range ensures low reflections across the entire lens surface. The GRIN profile is realized by the formation of different densities of a single 3D-printed material (VeroClear) with a dielectric constant of $\epsilon_r = 2.7$ at the design frequency band. A cubic inserted with four connecting rods, forming a lattice unit cell with a periodicity of $p = 4.58$ mm ($0.2\lambda_0$), is simulated in the Ansys high-frequency structure simulator (HFSS) for this lens design [64]. The schematic of the unit cell is shown in Figure 9(b). The effective refractive index is calculated based on the effective medium theory [65], and the results match the filling ratio of the dielectric. By changing the length of the insert, the refractive index can be varied. The corresponding required size of the 3D-printed cube for the desired effective refractive index distribution is plotted in Figure 9(b). Note that the presented unit cell meets the needs in terms of dispersion for the intended operating bandwidth, which is from 12 to 15 GHz. For wider band lens designs, an all-dielectric 3D-printed material with a different volume percentage of the dielectric material in nanoscale patterns can be used.

To demonstrate the multibeam performance of the lens, an array of 2×2 patches is used as the feed antenna of the lens. The feed (patch subarray) consists of two square substrates with the same side length of 28 mm separated by a spacer with a thickness of 1 mm. Both substrate materials are Rogers RT/duroid 5880 with a thickness of 0.787 mm ($\epsilon_r = 2.2$, $\tan\delta = 0.0009$). Details of the feed antenna design can be found in [63] with some modifications on the dimensions to fit into this new lens antenna. The feed antenna and dielectric lens are simulated in the Ansys HFSS. The patch feed configuration is shown in Figure 10(a). The lens consists of five similar layers of subwavelength unit cells, making a thickness of $1\lambda_0$. The focal length of the lens for the feed at the center of the circular arc is 80 mm ($3.6\lambda_0$), corresponding to the boresight beam. A schematic of the 2D GRIN lens antenna structure is shown in Figure 10(b). The dielectric flat lens and patch arrays are mounted on a fixture for measurement purposes. The lens radius is 55 mm ($2.5\lambda_0$). The

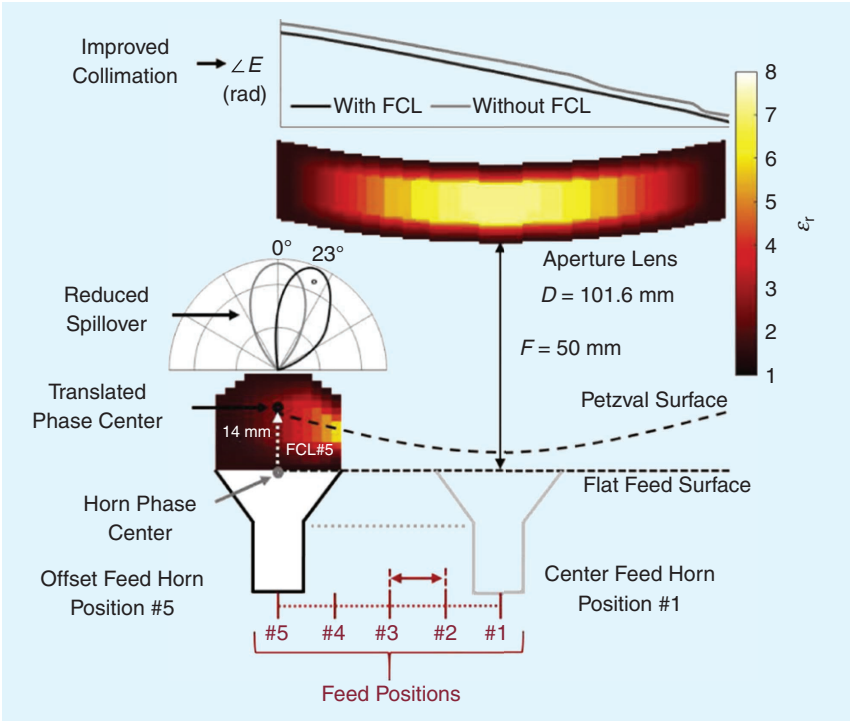

FIGURE 7. FCL concept [62]. w: with; w/o: without.

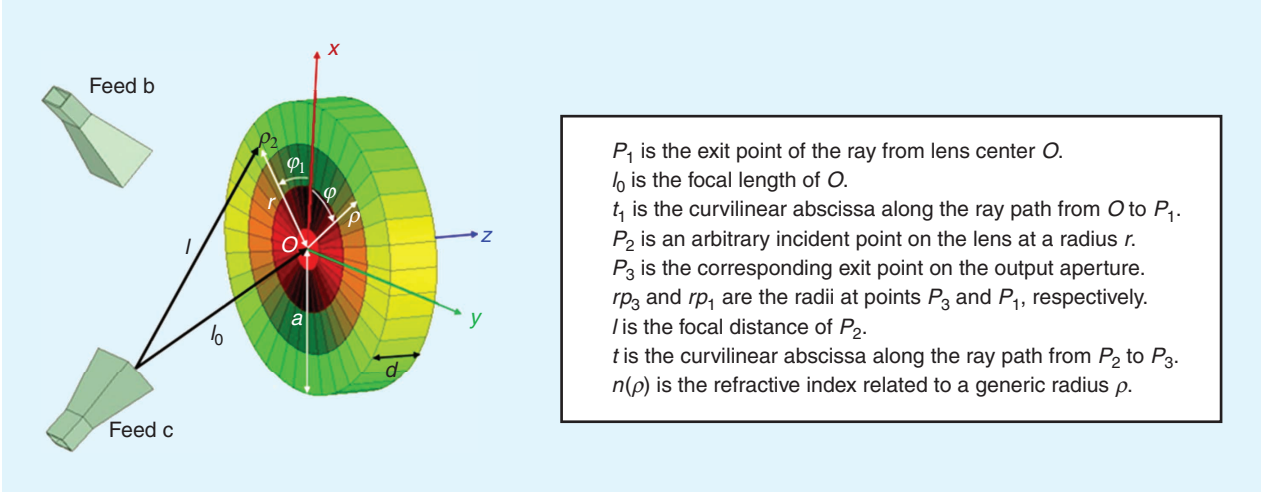

FIGURE 8. Configuration of multibeam lens with GRIN variation along both radial and azimuthal angle ϕ_1 directions (different colors on the lens aperture represent varied refractive indices) [63].

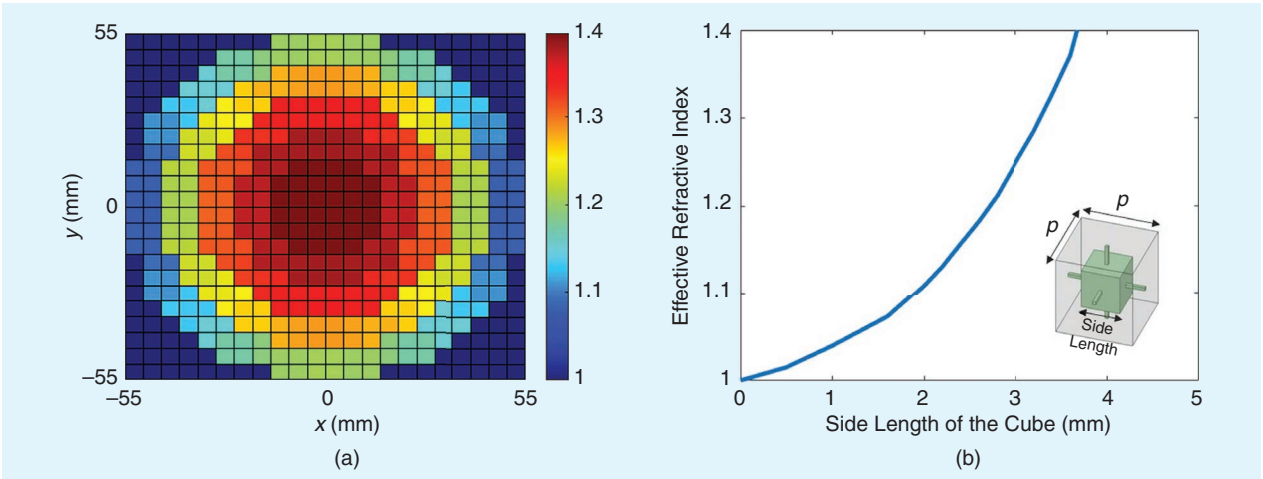

FIGURE 9. GRIN lens refractive index. (a) Calculated radial refractive index distribution. (Please note that the refractive index distribution of the lens is varying along both the radial and azimuthal directions.) (b) The effective refractive index of the unit cell for the normal incident. The unit cell period is 4.58 mm.

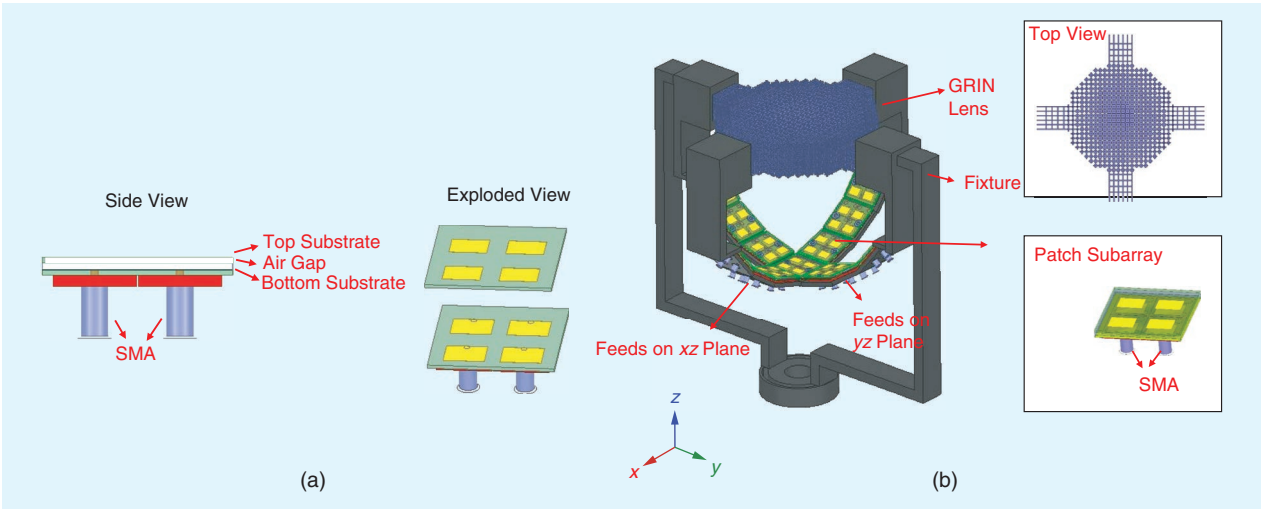

FIGURE 10. Configuration of the multibeam lens antenna. (a) Schematic of the patch feed (a side view and an exploded view are shown). (b) Schematic of the 2D multibeam GRIN lens antenna (a top view of the lens and a perspective view of the patch subarray are shown). SMA: SubMiniature version of A.

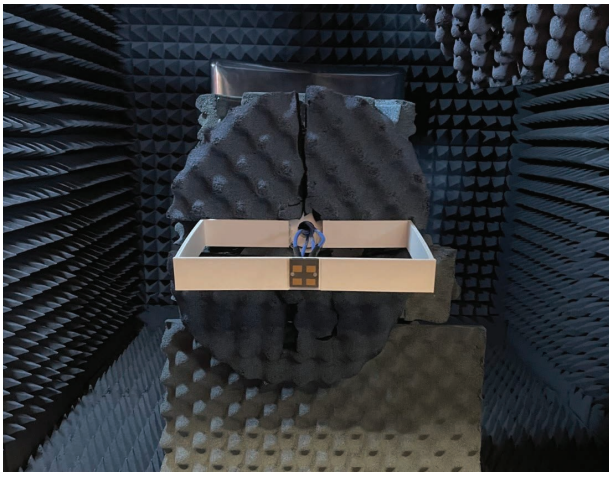

FIGURE 11. Prototype of the feed antenna in a fixture mounted in the anechoic chamber.

overall system's dimensions including the jig are 250 mm in width and 230 mm in length. This fixture primarily serves as a supporting structure without influencing the lens performance.

MEASURED RESULTS OF THE 3D-PRINTED 2D MULTIBEAM FLAT GRIN LENS

To verify the simulation results of the lens antenna, a prototype of the design is fabricated and measured in an anechoic chamber. First, several prototypes of the patch feed are fabricated to realize the multibeam lens antenna. A prototype of the feed mounted in the anechoic chamber is given in Figure 11. The simulated and measured feed antenna results are shown in Figure 12. The S-parameters of only one single port are given because all four ports are identical. It is seen that the simulated and measured results agree well. The –10-dB input reflection coefficient bandwidth is 25.8% from 11.8 to 15.3 GHz. The port isolation is better than –18 dB across the band from 12 to 15

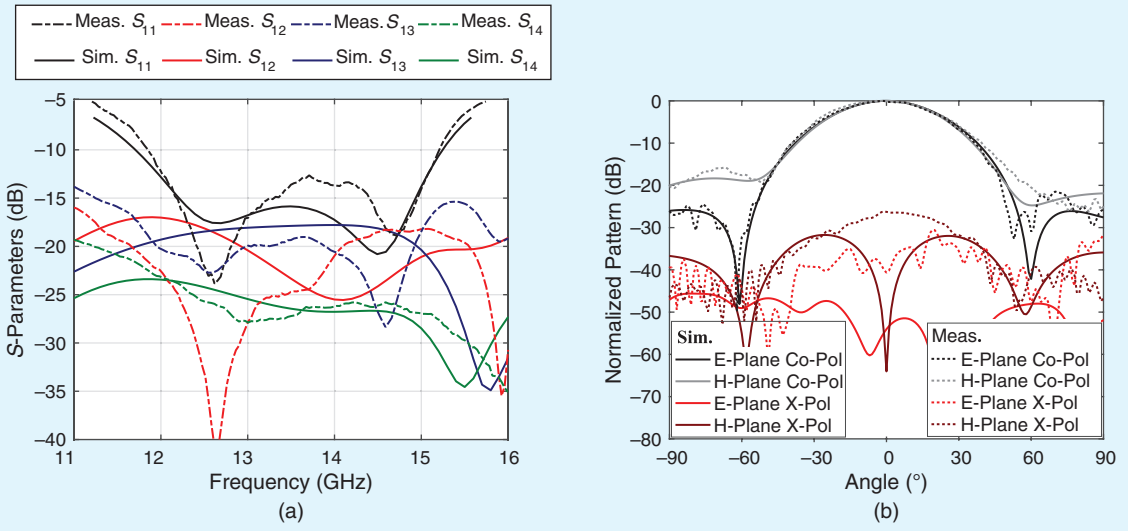

FIGURE 12. Simulated and measured results of the feed antenna. (a) Reflection coefficients and port isolations for port 1 versus frequency. (b) Simulated and measured normalized radiation patterns at 13.5 GHz. Co-pol: copolarized; X-pol: cross-polarized.

GHz. Figure 12(b) shows the simulated and measured copolarized and cross-polarized radiation patterns of the feed antenna along the E-plane and H-plane at 13.5 GHz. The peak realized gain is 13.4 dBi. The 10-dB beamwidths for both the E-plane and H-plane radiation patterns are about 70° with a cross-polarization level remaining below –30 dB at 13.5 GHz.

A lens is 3D printed based on the different sizes of dielectric cubes to achieve the desired GRIN profile. Thirteen feed array antennas are placed on the circular locus in both the *xz* plane and *yz* plane to realize the 2D multibeam performance of the lens antenna. It is to be noted that diagonal beam steering of the lens antenna in all different azimuthal cutting planes is possible by placing more feeds along the diagonal line of the lens. A 3D-printed fixture made of polymer is used to hold the lens and feeds in the correct position and mount the whole configuration on the test range. The lens is extended on four sides to accommodate it in the fixture. The whole configuration of the 2D GRIN lens antenna, the antenna prototype mounted in the test fixture, and the lens antenna under test are shown in Figure 13.

The reflection coefficients and port isolations of the lens antenna are measured using an Agilent Network Analyzer N5225A, and the results stay below –10 dB across the band, which demonstrates that the lens does not have much effect on the return loss of the feeding arrays. The radiation patterns of the multibeam lens antenna in the scanning planes are plotted in Figure 14. The simulated and measured radiation patterns are in good agreement. The radiation patterns are stable across the band. The plots show that the GRIN lens antenna enables a 2D angular coverage with a 90° scanning range and a scan loss of less than 2.4 dB across the band. Seven beams are generated in each plane. The pattern intersects at about –3.5 dB. The SLLs stay below –10 dB across the band for all of the angles. The measured peak realized gain is obtained by using gain comparison techniques.

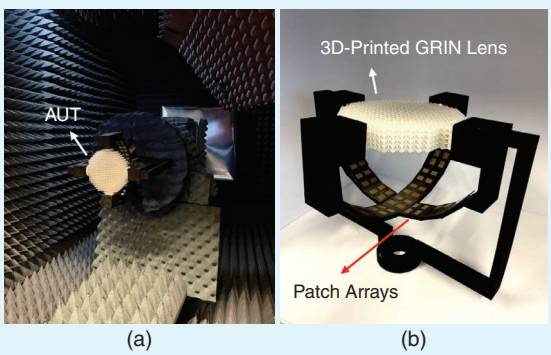

FIGURE 13. Photographs of antenna measurement. (a) The prototype in the anechoic chamber. (b) Fabricated prototype. AUT: antenna under test.

The simulated and measured peak realized gains across the frequency band for the beams in the *xz* plane are given in Figure 15. The results for the *yz* plane are not shown for brevity. This work presents a similar performance in terms of gain and bandwidth compared with our previous work [63]. The beam-scanning losses in the operating band are 0.4–1.8 dB and 0.7–2.4 dB in the *xz* and *yz* planes, respectively. This is almost 1.5 dB less than the results reported in [63]. The aperture efficiency is between 35% and 60% from 12 to 15 GHz for all of the angles. The lowest value corresponds to the gain drop at 15 GHz due to the limited bandwidth of the feed. The measured cross-polarization levels stay below –30 dB over the entire range for all of the beams across the band. The patterns are not shown here for conciseness.

A comparison of the radiation performance of the proposed multibeam flat GRIN lens with other reported flat lens designs is presented in Table 1. The lenses in [59], [66], and [67] have relatively small scanning ranges and low aperture

efficiencies that are below 40%. On the other hand, the designs in [60] and [62] achieve a wider scanning range, but they suffer from high scanning losses. In addition, the lens in [60] has a low aperture efficiency of below 30%. A flat GRIN lens with a high aperture efficiency and a wide scanning range is reported in [63]. The proposed design in this work demonstrates a comparable scanning range and an aperture efficiency as compared to [63], but it has smaller scanning losses and lower SLLs.

FUTURE CHALLENGES

The deployment of multibeam GRIN lens antennas for SatCom represents a promising era of connectivity, yet several challenges exist, demanding innovative solutions to unlock their

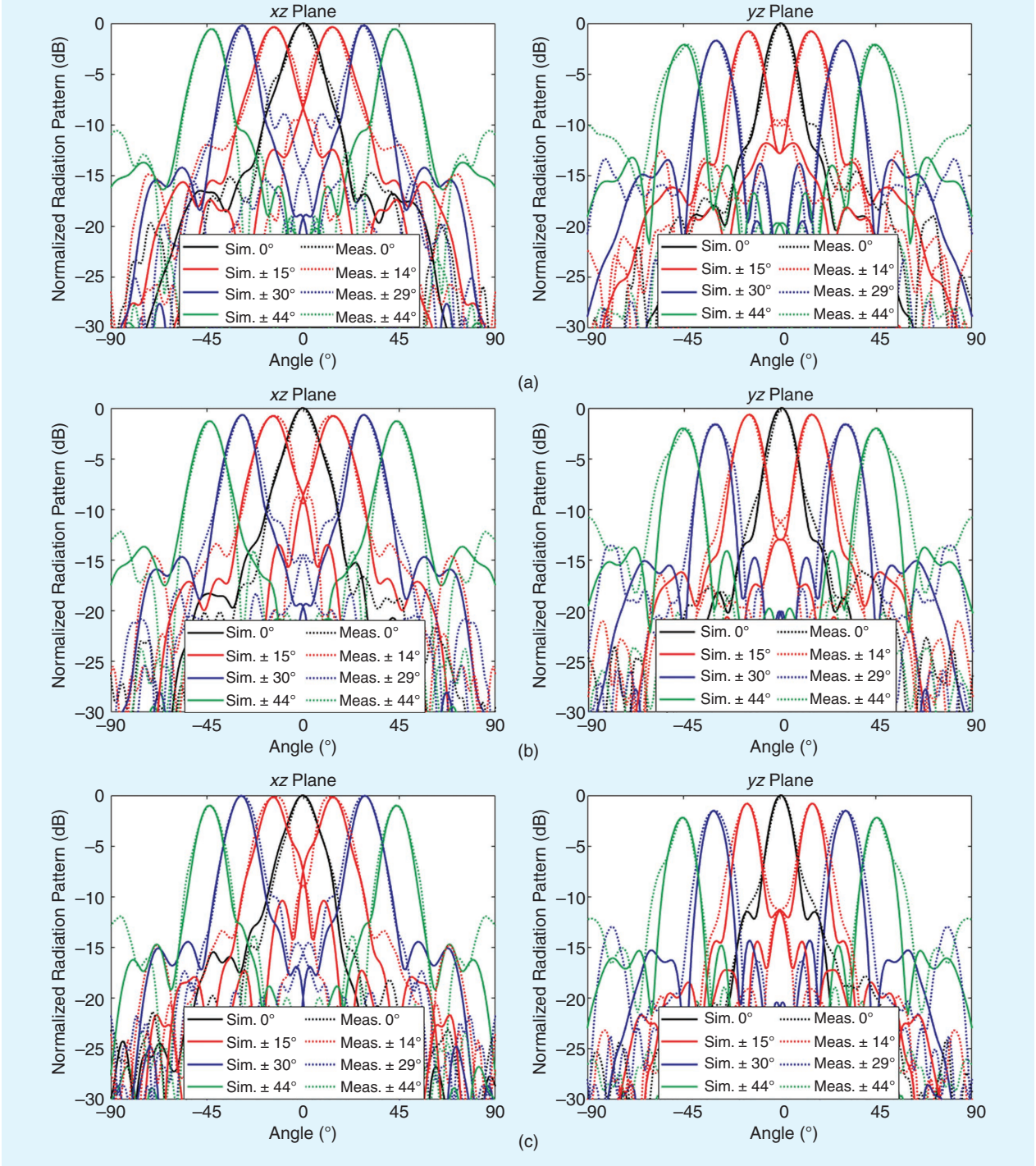

FIGURE 14. Simulated (solid lines) and measured (dashed lines) normalized radiation patterns of the multibeam lens antenna at (a) 12 GHz, (b) 13.5 GHz, and (c) 15 GHz.

TABLE 1. COMPARISON WITH OTHER REPORTED DESIGNS.

Ref.	Frequency (GHz)	Technology	SLL (dB)	Scan Loss (dB)	Beam Range	Aperture Efficiency (%)
[59]	45–110	3D-printed SLA	–5	8	±30°	19–36
[60]	60–77	CNC machine Rogers TMM6	–3.5	4.6	±48°	9.5–27.6
[62]	12–18	PCB Rogers AD250, AD350, TC600	–14	5.5	±53°	21–74
[63]	12–15	PCB Rogers 4003	–7.5	3.4	±46°	22–66.4
[66]	26.6–30	PCB Rogers 4003	–18.4	3.7	±27°	<24.5
[67]	12–18	3D-printed PLA	–11	0.5	±15	22–49
This work	12–15	3D-printed ABS	–10	2.4	±45°	35–60

SLA: stereolithography; PLA: polylactic acid; ABS: acrylonitrile butadiene styrene; CNC: computer numerical control.

full potential. Traditionally, flat multibeam GRIN lens antennas face limitations in their ability to achieve wide scanning angles while maintaining high efficiencies and low SLLs. One key aspect of overcoming this challenge lies in optimizing the design of the GRIN lens structure itself. By carefully tailoring the refractive index profile and geometry of the lens, antenna engineers can mitigate aberrations and achieve a wider field of view without sacrificing key performance metrics [41]. Additionally, advancements in metamaterials offer promising solutions for enhancing the gain and the efficiency of the GRIN lenses through the design of artificial dielectrics that allow low reflection and insertion losses [66].

Another key challenge is achieving a compact design, making it essential to minimize both the lens thickness and focal length. A shorter focal length can lead to significant phase and amplitude errors, potentially compromising the gain and the efficiency. Thus, there exists a tradeoff between the size and the performance of lens antennas.

Continuous beam scanning and tracking represent another frontier in enhancing the performance of SatCom systems. Developing seamless tracking capabilities is essential to ensure uninterrupted communication and optimized resource allocation in dynamic environments [42]. Finally, there is always a need to establish cost-effective methods for fabricating lenses with high precision. While 3D printing demonstrates considerable potential, the technology and materials to produce high-performance GRIN lenses are currently in the process of development.

The design of flat multibeam GRIN lens antennas for SatCom faces significant challenges. Addressing these challenges demands collaborative efforts from researchers, engineers, and industry stakeholders to push the boundaries of innovation in SatCom technology.

CONCLUSIONS

Technology advances for different flat GRIN lens antennas are discussed in this article. In particular, a multibeam GRIN lens antenna with a wide angular coverage and a high aperture efficiency at the Ku band operating from 12 to 15 GHz is presented. The feed elements are placed on two circular feed trajectories creating 13 beams covering from -45° to $+45^{\circ}$ in two planes allowing a 2D angular coverage. The measured peak realized gain is 22 dBi. The developed lens antenna is suitable for applications in which high-gain multibeam antennas are demanded.

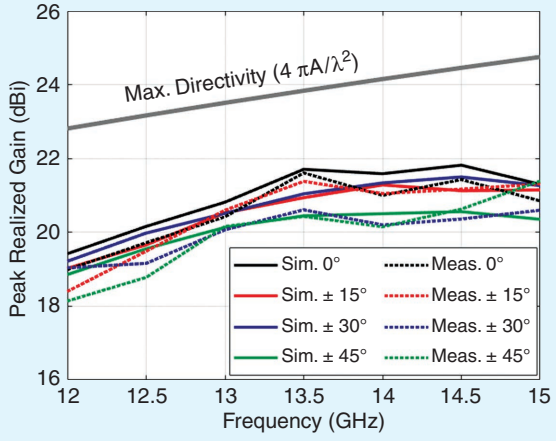

FIGURE 15. Simulated and measured peak realized gains across the frequency band.

AUTHOR INFORMATION

Maral Ansari (maral.ansari@csiro.au) is a research engineer at CSIRO Space and Astronomy, Marsfield, NSW 2122, Australia. She is a Member of IEEE.

Lizhao Song (lizhao.song@uts.edu.au) is a chancellor's research fellow at the Global Big Data Technologies Centre, University of Technology Sydney, 2007 Ultimo, NSW 2122, Australia. Her research interests include transmitarray antennas, lens antennas, and metasurfaces. She is a Member of IEEE.

Pei-Yuan Qin (peiyuan.qin@uts.edu.au) is an associate professor at the Global Big Data Technologies Centre, University of

Technology Sydney, 2007 Ultimo, NSW 2122, Australia. He is a Senior Member of IEEE.

Stephanie L. Smith (stephanie.smith@csiro.au) is head of Australia Telescope National Facility Instrumentation at CSIRO Space and Astronomy, Marsfield, NSW 2122, Australia. She is a Member of IEEE.

Y. Jay Guo (jay.guo@uts.edu.au) is a distinguished professor and the director of the Global Big Data Technologies Centre, University of Technology Sydney, 2007 Ultimo, NSW 2122, Australia. He is a Fellow of IEEE.

REFERENCES

[1] O. Kodheli et al., "Satellite communications in the new space era: A survey and future challenges," *IEEE Commun. Surveys Tuts.*, vol. 23, no. 1, pp. 70–109, 1st. Quart. 2021, doi: 10.1109/COMST.2020.3028247.

[2] Y. J. Guo, M. Ansari, and N. J. G. Fonseca, "Circuit type multiple beamforming networks for antenna arrays in 5G and 6G terrestrial and non-terrestrial networks," *IEEE J. Microwaves*, vol. 1, no. 3, pp. 704–722, Jul. 2021, doi: 10.1109/JMW.2021.3072873.

[3] J. Lee et al., "Phased array featuring independent, simultaneous beamsteering for widely separated mmwave dual-band using compact, low-loss, selective coupler," *IEEE Trans. Antennas Propag.*, vol. 72, no. 1, pp. 365–374, Jan. 2024, doi: 10.1109/TAP.2023.3331777.

[4] M. Liu, F. Lin, and H. J. Sun, "Broadband frequency-independent beamforming networks for multibeam antenna arrays," *IEEE Antennas Wireless Propag. Lett.*, vol. 22, no. 10, pp. 2397–2401, Oct. 2023, doi: 10.1109/LAWP.2023.3289146.

[5] J. Butler, "Beam-forming matrix simplifies design of electronically scanned antennas," *Electron. Des.*, vol. 9, no. 8, pp. 170–173, 1961.

[6] M. Ansari, H. Zhu, N. Shariati, and Y. J. Guo, "Compact planar beamforming array with endfire radiating elements for 5G applications," *IEEE Trans. Antennas Propag.*, vol. 67, no. 11, pp. 6859–6869, Nov. 2019, doi: 10.1109/TAP.2019.2925179.

[7] J.-W. Lian, Y.-L. Ban, Q.-L. Yang, B. Fu, Z.-F. Yu, and L.-K. Sun, "Planar millimeter-wave 2-D beam-scanning multibeam array antenna fed by compact SIW beam-forming network," *IEEE Trans. Antennas Propag.*, vol. 66, no. 3, pp. 1299–1310, Mar. 2018, doi: 10.1109/TAP.2018.2797873.

[8] J. Blass, "Multidirectional antenna - A new approach to stacked beams," in *Proc. IRE Int. Conv. Rec.*, Piscataway, NJ, USA: IEEE Press, 1966, pp. 48–50, doi: 10.1109/IRECON.1960.1150892.

[9] C. Tsokos et al., "Analysis of a multibeam optical beamforming network based on Blass matrix architecture," *J. Lightwave Technol.*, vol. 36, no. 16, pp. 3354–3372, Aug. 2018, doi: 10.1109/JLT.2018.2841861.

[10] N. J. G. Fonseca, "Printed S-band 4 × 4 Nolen matrix for multiple beam antenna applications," *IEEE Trans. Antennas Propag.*, vol. 57, no. 6, pp. 1673–1678, Jun. 2009, doi: 10.1109/TAP.2009.2019919.

[11] T. Djerafi, N. J. G. Fonseca, and K. Wu, "Planar Ku-band 4 × 4 Nolen matrix in SIW technology," *IEEE Trans. Microwave Theory Tech.*, vol. 58, no. 2, pp. 259–266, Feb. 2010, doi: 10.1109/TMTT.2009.2037866.

[12] C. A. Guo and Y. J. Guo, "A general approach for synthesizing multibeam antenna arrays employing generalized joined coupler matrix," *IEEE Trans. Antennas Propag.*, vol. 70, no. 9, pp. 7556–7564, Sep. 2022, doi: 10.1109/TAP.2022.3153037.

[13] C. A. Guo, Y. J. Guo, and J. Yuan, "Multibeam receiving antennas employing generalized joined coupler matrix," *IEEE Trans. Antennas Propag.*, vol. 72, no. 1, pp. 424–432, Jan. 2024, doi: 10.1109/TAP.2023.3330634.

[14] Y. J. Guo, M. Ansari, R. W. Ziolkowski, and N. J. G. Fonseca, "Quasi-optical multi-beam antenna technologies for B5G and 6G mmwave and THz networks: A review," *IEEE Open J. Antennas Propag.*, vol. 2, pp. 807–830, 2021, doi: 10.1109/OJAP.2021.3093622.

[15] Y. J. Cheng, W. Hong, and K. Wu, "Millimeter-wave substrate integrated waveguide multibeam antenna based on the parabolic reflector principle," *IEEE Trans. Antennas Propag.*, vol. 56, no. 9, pp. 3055–3058, Sep. 2008, doi: 10.1109/TAP.2008.928812.

[16] X. Qi, F. Li, H. Zhao, Z. Xu, and H. Li, "Steerable simultaneous multibeam antenna based on reconfigurable reflectarray," *IEEE Antennas Wireless Propag. Lett.*, vol. 22, no. 8, pp. 2037–2041, Aug. 2023, doi: 10.1109/LAWP.2023.3273428.

[17] J.-W. Lian, Y.-L. Ban, and Y. J. Guo, "Wideband dual-layer huygens' metasurface for high-gain multibeam array antennas," *IEEE Trans. Antennas Propag.*, vol. 69, no. 11, pp. 7521–7531, Nov. 2021, doi: 10.1109/TAP.2021.3076669.

[18] Y. Wen, P.-Y. Qin, S. Maci, and Y. J. Guo, "Low-profile multibeam antenna based on modulated metasurface," *IEEE Trans. Antennas Propag.*, vol. 71, no. 8, pp. 6568–6578, Aug. 2023, doi: 10.1109/TAP.2023.3281677.

[19] P. Naseri, S. A. Matos, J. R. Costa, C. A. Fernandes, and N. J. G. Fonseca, "Dual-band dual-linear-to-circular polarization converter in transmission mode application to Ku-band satellite communications," *IEEE Trans. Antennas Propag.*, vol. 66, no. 12, pp. 7128–7137, Dec. 2018, doi: 10.1109/TAP.2018.2874680.

[20] L. Song, P.-Y. Qin, H. Zhu, and J. Du, "Wideband conformal transmitarrays for E-band multi-beam applications," *IEEE Trans. Antennas Propag.*, vol. 70, no. 11, pp. 10,417–10,425, Nov. 2022, doi: 10.1109/TAP.2022.3191412.

[21] K. Duan, K. Chen, Y. Zheng, T. Jiang, J. Zhao, and Y. Feng, "Low-scattering and dual-polarized reconfigurable reflectarray antenna based on absorptive and active coding metasurfaces," *IEEE Trans. Antennas Propag.*, vol. 72, no. 3, pp. 2490–2501, Mar. 2024, doi: 10.1109/TAP.2024.3356060.

[22] Y. Hu, W. Hong, and Z. H. Jiang, "A multibeam folded reflectarray antenna with wide coverage and integrated primary sources for millimeter-wave massive MIMO applications," *IEEE Trans. Antennas Propag.*, vol. 66, no. 12, pp. 6875–6882, Dec. 2018, doi: 10.1109/TAP.2018.2871747.

[23] S. Lei, G. Wei, K. Han, X. Li, and T. Qiu, "A simple method to design wideband circularly polarized spherical multibeam Luneburg lens antenna," *IEEE Antennas Wireless Propag. Lett.*, vol. 21, no. 7, pp. 1423–1427, Jul. 2022, doi: 10.1109/LAWP.2022.3170492.

[24] Q. Wu et al., "Transformation optics inspired multibeam lens antennas for broadband directive radiation," *IEEE Trans. Antennas Propag.*, vol. 61, no. 12, pp. 5910–5922, Dec. 2013, doi: 10.1109/TAP.2013.2282905.

[25] F. Holt and A. Mayer, "A design procedure for dielectric microwave lenses of large aperture ratio and large scanning angle," *IRE Trans. Antennas Propag.*, vol. 5, no. 1, pp. 25–30, Jan. 1957, doi: 10.1109/TAP.1957.1144474.

[26] D. G. Bodnar, "Lens antennas," in *The Handbook of Antenna Design*, vol. 1, A. W. Rudge, K. Milne, A. D. Olver, and P. Knight, Eds., London, U.K.: Peter Peregrinus, 1986, pp. 1–31.

[27] H. F. Ma and T. J. Cui, "Three-dimensional broadband and broad-angle transformation-optics lens," *Nature Commun.*, vol. 1, no. 1, 2010, Art. no. 124, doi: 10.1038/ncomms1126.

[28] Q.-W. Lin and H. Wong, "A low-profile and wideband lens antenna based on high-refractive-index metasurface," *IEEE Trans. Antennas Propag.*, vol. 66, no. 11, pp. 5764–5772, Nov. 2018, doi: 10.1109/TAP.2018.2866528.

[29] A. Peebles, "A dielectric bifocal lens for multibeam antenna applications," *IEEE Trans. Antennas Propag.*, vol. 36, no. 5, pp. 599–606, May 1988, doi: 10.1109/8.192135.

[30] C. A. Fernandes, E. B. Lima, and J. R. Costa, "Dielectric lens antennas," in *Handbook Antenna Technologies*, Z. Chen, D. Liu, H. Nakano, X. Qing, and T. Zwick, Eds., Singapore: Springer-Verlag, 2016, pp. 1001–1064.

[31] C. M. C. Martin, W. Hu, and D. Cavallo, "Design of wideband flat artificial dielectric lenses at mmwave frequencies," *IEEE Trans. Antennas Propag.*, vol. 72, no. 2, pp. 1418–1428, Feb. 2024, doi: 10.1109/TAP.2024.3357992.

[32] D. H. Archer, "Lens-fed multiple-beam arrays," *Microw. J.*, vol. 27, p. 171, Sep. 1984.

[33] E. B. Lima, S. A. Matos, J. R. Costa, C. A. Fernandes, and N. J. G. Fonseca, "Circular polarization wide-angle beam steering at Ka-band by in-plane translation of a plate lens antenna," *IEEE Trans. Antennas Propag.*, vol. 63, no. 12, pp. 5443–5455, Dec. 2015, doi: 10.1109/TAP.2015.2484419.

[34] Y. Su and Z. N. Chen, "A flat dual-polarized transformation-optics beamscanning Luneburg lens antenna using PCB-stacked gradient index metamaterials," *IEEE Trans. Antennas Propag.*, vol. 66, no. 10, pp. 5088–5097, Oct. 2018, doi: 10.1109/TAP.2018.2858209.

[35] A. Mozharovskiy, A. Artemenko, A. Sevastyanov, V. Ssorin, and R. Maslennikov, "Beam-steerable integrated lens antenna with waveguide feeding system for 71–76/81–86 GHz point-to-point applications," in *Proc. 10th Eur. Conf. Antennas Propag. (EuCAP)*, Piscataway, NJ, USA: IEEE Press, 2016, pp. 1–5, doi: 10.1109/EuCAP.2016.7481774.

[36] J. R. Costa, M. G. Silveirinha, and C. A. Fernandes, "Evaluation of a double-shell integrated scanning lens antenna," *IEEE Antennas Wireless Propag. Lett.*, vol. 7, pp. 781–784, Oct. 2008, doi: 10.1109/LAWP.2008.2008403.

[37] S. Zhang, R. K. Arya, W. G. Whittow, D. Cadman, R. Mittra, and J. Vardaxoglou, "Ultra-wideband flat metamaterial GRIN lenses assisted with additive manufacturing technique," *IEEE Trans. Antennas Propag.*, vol. 69, no. 7, pp. 3788–3799, Jul. 2020, doi: 10.1109/TAP.2020.3044586.

[38] F. Maggiorelli, A. Paraskevopoulos, J. Vardaxoglou, M. Albani, and S. Maci, "Profile inversion and closed form formulation of compact GRIN lenses," *IEEE Open J. Antennas Propag.*, vol. 2, pp. 315–325, 2021, doi: 10.1109/OJAP.2021.3059468.

[39] Q. Lou and Z. N. Chen, "Flat-focal-plane dual-metasurface lens for low scan loss and sidelobe level of a metalens antenna," *IEEE Trans. Antennas Propag.*, vol. 70, no. 10, pp. 9849–9854, Oct. 2022, doi: 10.1109/TAP.2022.3177558.

[40] Y. Li, L. Ge, M. Chen, Z. Zhang, Z. Li, and J. Wang, "Multibeam 3-D-printed Luneburg lens fed by magnetoelectric dipole antennas for millimeter-wave

MIMO applications," *IEEE Trans. Antennas Propag.*, vol. 67, no. 5, pp. 2923–2933, May 2019, doi: 10.1109/TAP.2019.2899013.
[41] C. Mateo-Segura, A. Dyke, H. Dyke, S. Haq, and Y. Hao, "Flat Luneburg lens via transformation optics for directive antenna applications," *IEEE Trans. Antennas Propag.*, vol. 62, no. 4, pp. 1945–1953, Apr. 2014, doi: 10.1109/TAP.2014.2302004.
[42] L. Song, T. Zhang, J.-X. Lai, Y. Yang, and J. Du, "A 180-GHz to 220-GHz wideband transmitarray with wide-angle beam steering for intersatellite communications," *IEEE Trans. Antennas Propag.*, vol. 72, no. 1, pp. 950–955, Jan. 2024, doi: 10.1109/TAP.2023.3324421.
[43] J. Budhu and Y. Rahmat-Samii, "3D-printed inhomogeneous dielectric lens antenna diagnostics: A tool for assessing lenses misprinted due to fabrication tolerances," *IEEE Antennas Propag. Mag.*, vol. 62, no. 4, pp. 49–61, Apr. 2020, doi: 10.1109/MAP.2019.2946566.
[44] K. Liu, C. Zhao, S.-W. Qu, Y. Chen, J. Hu, and S. Yang, "A 3-D-printed multibeam spherical lens antenna with ultrawide-angle coverage," *IEEE Antennas Wireless Propag. Lett.*, vol. 20, no. 3, pp. 411–415, Mar. 2021, doi: 10.1109/LAWP.2021.3054042.
[45] C. Wang, Y. Xia, G. Guo, M. Nasir, and Q. Zhu, "Ellipsoidal Luneburg lens binary array for wide-angle scanning," *IEEE Trans. Antennas Propag.*, vol. 68, no. 7, pp. 5702–5707, Jul. 2020, doi: 10.1109/TAP.2020.2969875.
[46] M. Liang, W.-R. Ng, K. Chang, K. Gbele, M. E. Gehm, and H. Xin, "A 3-D Luneburg lens antenna fabricated by polymer jetting rapid prototyping," *IEEE Trans. Antennas Propag.*, vol. 62, no. 4, pp. 1799–1807, Apr. 2014, doi: 10.1109/TAP.2013.2297165.
[47] Y.-H. Lou, Y.-X. Zhu, G.-F. Fan, W. Lei, W.-Z. Lu, and X.-C. Wang, "Design of Ku-band flat Luneburg lens using ceramic 3-D printing," *IEEE Antennas Wireless Propag. Lett.*, vol. 20, no. 2, pp. 234–238, Feb. 2020, doi: 10.1109/LAWP.2020.3046489.
[48] Y. Guo and S. Barton, "Phase correcting zonal reflector incorporating rings," *IEEE Trans. Antennas Propag.*, vol. 43, no. 4, pp. 350–355, Apr. 1995, doi: 10.1109/8.376031.
[49] D. N. Black and J. C. Wiltse, "Millimeter-wave characteristics of phase-correcting Fresnel zone plates," *IEEE Trans. Microwave Theory Tech.*, vol. 35, no. 12, pp. 1122–1129, Dec. 1987, doi: 10.1109/TMTT.1987.1133826.
[50] H. D. Hristov and M. H. Herben, "Millimeter-wave Fresnel-zone plate lens and antenna," *IEEE Trans. Microwave Theory Techn.*, vol. 43, no. 12, pp. 2779–2785, Dec. 1995, doi: 10.1109/22.475635.
[51] A. O. Bah, P.-Y. Qin, R. W. Ziolkowski, Q. Cheng, and Y. J. Guo, "Realization of an ultra-thin metasurface to facilitate wide bandwidth, wide angle beam scanning," *Sci. Rep.*, vol. 8, no. 1, 2018, Art. no. 4761, doi: 10.1038/s41598-018-23288-4.
[52] W. Yang, K. Chen, J. Zhao, T. Jiang, and Y. Feng, "A wideband high-efficiency transmit-reflect-array antenna for bidirectional radiations with distinct circular polarizations based on a metasurface," *IEEE Trans. Antennas Propag.*, vol. 71, no. 4, pp. 3695–3700, Apr. 2023, doi: 10.1109/TAP.2023.3249911.
[53] K. T. Pham, A. Clemente, D. Blanco, and R. Sauleau, "Dual-circularly polarized high-gain transmitarray antennas at Ka-band," *IEEE Trans. Antennas Propag.*, vol. 68, no. 10, pp. 7223–7227, Oct. 2020, doi: 10.1109/TAP.2020.2996680.
[54] H. Yu, J. Su, Z. Li, and F. Yang, "A novel wideband and high-efficiency electronically scanning transmitarray using transmission metasurface polarizer," *IEEE Trans. Antennas Propag.*, vol. 70, no. 4, pp. 3088–3093, Apr. 2022, doi: 10.1109/TAP.2021.3137414.
[55] Q. Ma, C. B. Shi, T. Y. Chen, M. Q. Qi, Y. B. Li, and T. J. Cui, "Broadband metamaterial lens antennas with special properties by controlling both refractive-index distribution and feed directivity," *J. Optics*, vol. 20, no. 4, 2018, Art. no. 045101, doi: 10.1088/2040-8986/aaacbf.
[56] K. Kelleher, "Dielectric lens for microwave," *Electronics*, vol. 8, pp. 142–145, 1955.
[57] A. Paraskevopoulos, F. Maggiorelli, M. Albani, and S. Maci, "Radial GRIN lenses based on the solution of a regularized ray congruence equation," *IEEE Trans. Antennas Propag.*, vol. 70, no. 2, pp. 888–899, Feb. 2022, doi: 10.1109/TAP.2021.3111315.
[58] A. Papathanasopoulos, Y. Rahmat-Samii, N. C. Garcia, and J. D. Chisum, "A novel collapsible flat-layered metamaterial gradient-refractive-index lens antenna," *IEEE Trans. Antennas Propag.*, vol. 68, no. 3, pp. 1312–1321, Mar. 2020, doi: 10.1109/TAP.2019.2944546.
[59] S. Manafi, J. F. González, and D. S. Filipovic, "Design of a perforated flat Luneburg lens antenna array for wideband millimeter-wave applications," in *Proc. 13th Eur. Conf. Antennas Propag. (EuCAP)*, 2019, pp. 1–5.
[60] M. Imbert, A. Papió, F. De Flaviis, L. Jofre, and J. Romeu, "Design and performance evaluation of a dielectric flat lens antenna for millimeter-wave applications," *IEEE Antennas Wireless Propag. Lett.*, vol. 14, pp. 342–345, Oct. 2015, doi: 10.1109/LAWP.2014.2363596.
[61] J. Melendro-Jimenez, P. Sanchez-Olivares, A. Tamayo-Dominguez, X. Sun, and J. M. Fernandez-Gonzalez, "3D printed directive beam-steering antenna based on gradient index flat lens with an integrated polarizer for dual circular polarization at w-band," *IEEE Trans. Antennas Propag.*, vol. 71, no. 1, pp. 1059–1064, Jan. 2023, doi: 10.1109/TAP.2022.3217177.
[62] N. Garcia, W. Wang, and J. Chisum, "Feed corrective lenslets for enhanced beamscan in flat lens antenna systems," *Opt. Express*, vol. 30, no. 8, pp. 13,047–13,058, 2022, doi: 10.1364/OE.449130.
[63] L. Song, M. Ansari, P.-Y. Qin, S. Maci, J. Du, and Y. J. Guo, "Two-dimensional wide-angle multibeam flat GRIN lens with a high aperture efficiency," *IEEE Trans. Antennas Propag.*, vol. 71, no. 10, pp. 8018–8029, Oct. 2023, doi: 10.1109/TAP.2023.3298143.
[64] "Ansys HFSS — 3D high frequency simulation software," Ansys, Canonsburg, PA, USA, 2023. [Online]. Available: https://www.ansys.com/products/electronics/ansys-hfss
[65] R. Ziolkowski, "Design, fabrication, and testing of double negative metamaterials," *IEEE Trans. Antennas Propag.*, vol. 51, no. 7, pp. 1516–1529, Jul. 2003, doi: 10.1109/TAP.2003.813622.
[66] M. Jiang, Z. N. Chen, Y. Zhang, W. Hong, and X. Xuan, "Metamaterial-based thin planar lens antenna for spatial beamforming and multibeam massive MIMO," *IEEE Trans. Antennas Propag.*, vol. 65, no. 2, pp. 464–472, Feb. 2017, doi: 10.1109/TAP.2016.2631589.
[67] S. Zhang, R. K. Arya, S. Pandey, Y. Vardaxoglou, W. Whittow, and R. Mittra, "3D-printed planar graded index lenses," *IET Microwaves Antennas Propag.*, vol. 10, no. 13, pp. 1411–1419, 2016, doi: 10.1049/iet-map.2016.0013.